SUPPLEMENTAL MATERIAL
Carbon bonding controls the thermal conductivity mechanisms in high entropy carbide thin films

C.M. Rost,[1,2] T. Borman,[3] M.D. Hossain,[3] M. Lim,[4] K.F. Quiambao-Tomko,[5] J. Tomko,[5] D.W. Brenner,[4] J-P. Maria,[3] and Patrick E. Hopkins[1,5,6*]

[1] Department of Mechanical and Aerospace Engineering, University of Virginia, Charlottesville, VA 22904, USA.
[2] Current Address: Department of Physics and Astronomy, James Madison University, Harrisonburg, VA 22807, USA
[3] Department of Materials Science and Engineering, The Pennsylvania State University, State College, PA 16802, USA.
[4] Department of Materials Science and Engineering, North Carolina State University, Raleigh, NC 27695, USA.
[5] Department of Materials Science and Engineering, University of Virginia, Charlottesville, VA 22904, USA.
[6] Department of Physics, University of Virginia, Charlottesville, VA 22904, USA.

*e-mail: phopkins@virginia.edu

S1. Methods and details of TDTR analysis

All films were deposited on single-side polished c-plane sapphire substrates, cleaned with isopropanol and methanol followed by UV-ozone treatment for 10 minutes. $\mathrm{HfZrTaMoWC}_{1\text{-}x}$ samples were sputtered using a metal alloy target containing equimolar amounts of each element at 650 °C. Plasma was powered with a DC power supply set to 0.45 A constant current. Argon was fixed at 40 sccm and the pressure was set to 5 mTorr during the 5 minute pre-sputter phase. Methane was flowed for 2 minutes while sputtering then the shutter was opened and films were deposited. The total pressure was allowed to drift toward equilibrium for each deposition.

X-ray diffraction and reflectivity was measured on a Panalytical Empyrean using Cu radiation. Diffraction was measured at 45 kV/40 mA with a Bragg-Brentano HD incident optic using 1/2° divergence and 2° anti-scatter slits diffracted through a 1° anti-scatter slit fitted to a PIXcel3D detector operating in scanning line mode. X-ray reflectivity (XRR) was measured using the Bragg-Brentano HD incident optic with 1/8° divergence slit and 1/16° anti-scatter slit, reflected though a 0.05 mm anti-scatter slit into the PIXcel3D detector operating in receiving slit mode with 1 channel (0.055 mm). For the thin film series, we use XRR to measure the mass density.

Field-emission electron microscopy was conducted with a Zeiss Sigma FE-SEM. All images were taken with a 5 kV accelerating voltage and working distances of 2.5-3 mm through the In-lens secondary electron detector. X-ray photoelectron spectra were measured on a Phi Versaprobe II XPS using Al K-α radiation. Samples were sputtered for 5 minutes (15-20 nm) with a 3 kV Ar+ beam to remove any surface oxide layer. Ion and electron neutralization were used to prevent sample charging during the measurement process. C1s, Hf4f, Ta4f, W4f, Mo3p, and Zr3d spectra were collected for the respective samples in order to avoid peak overlaps.

Elastic moduli were measured with nanoindentation using a Bruker Hysitron TI-980 with Berkovich indenter. Tip to optic calibration was performed with polycarbonate while the tip area was calibrated with fused silica. The Olivar-Pharr method was implemented to extract the moduli data with a maximum applied load of 5.5 mN. The loading cycle durations were 5 s with a hold of 2 s at the maximum load. Nine indents were performed on each sample with each indent 20 μm apart. The actual elastic modulus of the samples was calculated using the following elastic modulus relationship between the indenter and the sample,[1]

$$\frac{1}{E_r} = \frac{1-\nu_i^2}{E_i} + \frac{1-\nu_s^2}{E_s}$$

Here, E_r is the reduced elastic modulus obtained from the load-displacement curve, ν_i and E_i are the Poisson's ratio and elastic modulus of the diamond indenter (assumed to be 0.07 and 1140 GPa, respectively) whereas ν_s and E_s are the Poisson's ratio and elastic modulus of the sample. We have assumed the Poisson's ratio of the sample to be 0.22, which is the rule of mixing average of binary carbides of the constituents of HEC6 in their stable structure.

Electrical conductivity was measured by the four-point probe technique using a Signatone probe head with a 1 mm probe spacings. A current of 4.5325 mA was sourced from a Keithley 2400 source meter and the voltage drop was measured with a Keithley 2182A nano-voltmeter. Measurements were taken at 5 points near the center of the sample and averaged. Volume resistivity was calculated with the geometry correction factors published by Smits for thin films on insulating substrates.

Thermal conductivity was measured using a two-color time-domain thermoreflectance (TDTR) setup with pump and probe wavelengths at 400 nm and 800 nm, respectively. A greater description of the physics behind this technique can be found in the literature.[2-4] Briefly, output from a pulsed, 800 nm wavelength Ti:Sapphire laser system (Spectra Physics Tsunami) at a frequency of 80 MHz and bandwidth of 10.5 nm, is split into the pump and probe paths. The pump path passes through an electro-optical modulator (EOM) with a tunable frequency between 0.1 and 10 MHz, then converted to 400 nm via a second harmonic generating BiB_3O_6 crystal. These pump pulses are then focused on the sample surface using a 10X infinity corrected microscope objective (Mitutoyo), creating a modulated heating event on the sample surface. The probe path is passed through a mechanical delay stage, incrementally varying the arrival time between the pump and probe. The back reflection of the probe is returned to a Si photodiode (Thorlabs DET10A) where the in-phase (X) and out-of-phase (Y) voltages are recorded through a lock-in amplifier, monitoring changes with respect to the modulated heating event from the pump. Thermal properties used in the radially symmetric, multilayer heat transfer model[2-4] to fit TDTR results to determine the thermal conductivities of the HEC films were found in the literature.[5-10]

We fit this aforementioned thermal model to both the in-phase signal and ratio of the in-phase to out-of-phase signals simultaneously to measure the thermal conductivity and volumetric heat capacity, C, of these thin films. The ratio and the in-phase signal offer different measurement sensitivities to κ and C, and thus by iterating between these two signals we can measure both of these properties. In a TDTR signal, the transient in-phase signal is related to the thermal response of the sample due to the impulse response from the laser. Since the ratio of the in-phase to out-of-phase voltage is related to the out of phase response, analyzing this ratio gains sensitivity to the decaying thermal wave established by the modulated heating event. These two thermal phenomena (impulse and modulated response) have different measurement sensitives to different thermophysical properties in the sample of interest. We have described this analysis in detail in our previous work,[11] but we not that this is only possible in our thin film series where the ratio offers different sensitivities to κ and C when the modulation frequency induces a thermal wave that has a decay length (thermal penetration depth) that is on the order or greater than the film thickness. If the sample is much thicker than the thermal penetration depth, than the modulated response (out-of-phase signal and ratio) become sensitive to the thermal effusivity of the sample, and thus a TDTR measurement is equally sensitive to κ and C, and so these parameters can not be decoupled. Therefore, for the thick $HfZrTaMoWC_{1-x}$ films, we use the values of C measured on the thin film.

We show TDTR sensitivity curves in Fig. S1 for the ratio and in-phase signals on the 2 and 6 sccm thin HEC films. These sensitivities are calculated using the technique presented by Costescu *et al.*[12] In general, the ratio is most sensitive to the thermal conductivity of the HEC films, more so than the thermal boundary conductances at either interface (G) or the heat capacity of the HEC. However, by analyzing the in-phase signal with the best fit values from the ratio fit as input, the increased relative sensitivity to C relative to κ compared to these sensitivities in the ratio fits allows for the determination of C of the HECs. We iterate back and forth between analysis of the ratio and in-phase signal until we converge on best fit κ and C for these thin HECs. Note, we have relatively low sensitivities to the thermal boundary conductances, and further, due to the lack of curvature of the thermal boundary conductance sensitivities in the in-phase signal, we are nearly completely insensitive to G in our in-phase analysis (note, the in-phase analysis involves normalizing the thermal model to the TDTR in-phase data, and thus when analyzing the in-phase data, TDTR measurements are only sensitive to thermophysical properties that change the slope or curvature of the TDTR data with pump-probe delay time). Thus, our reported values for κ and C are not obfuscated by the thermal boundary conductances at the Al/HEC and HEC/sapphire interfaces.

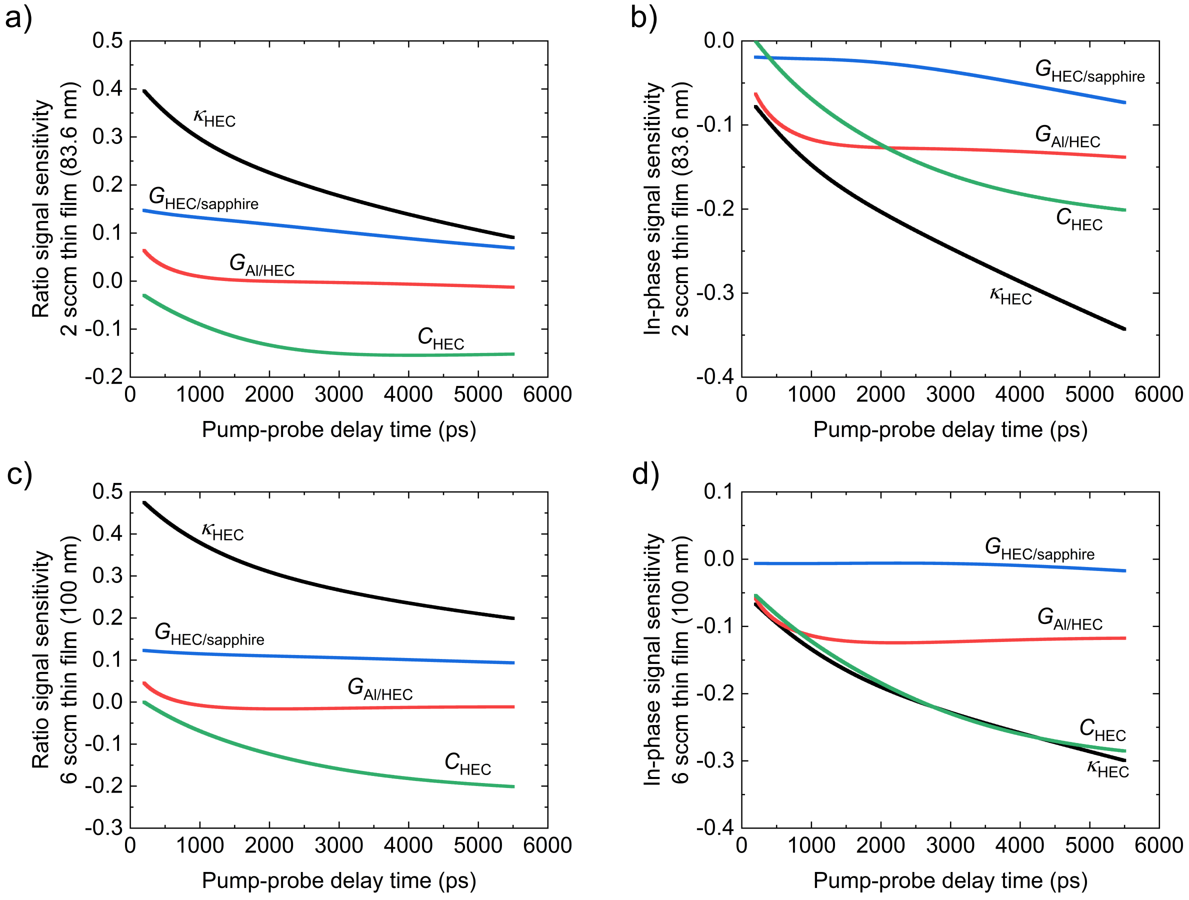

Figure S1: Sensitivities of our TDTR measurement to pertinent thermal properties of our Al/HEC/sapphire samples, including the thermal conductivity of the HEC (κ_{HEC}), the volumetric heat capacity of the HEC (C_{HEC}), and the thermal boundary conductances across the Al/HEC and HEC/sapphire interfaces ($G_{Al/HEC}$ and $G_{HEC/sapphire}$, respectively). We show these sensitivities for (a) the ratio response from the 2 sccm HEC thin film, (b) the in-phase response from the 2 sccm HEC thin film, (c) the ratio response from the 6 sccm thin film, and (d) the in-phase response from the 6 sccm thin film.

S2. HfZrTaMoWC$_{1-x}$ thin film details

Table S1. Primary thick film HfZrTaMoWC$_{1-x}$ sample set including methane parameters during deposition, thickness, electrical, and thermal conductivities.

CH_4 Flow Rate	% CH_4	Thickness	Electrical Conductivity	Thermal Conductivity
(sccm)		(μm)	($\mu\Omega^{-1}\cdot m^{-1}$)	($W\cdot m^{-1}\cdot K^{-1}$)
2	4.8	1.45 ± 0.02	0.48 ± 0.01	4.8 ± 0.7
4	9.1	1.52 ± 0.02	0.34 ± 0.01	3.6 ± 0.4
6	13	1.81 ± 0.03	0.12 ± 0.01	2.5 ± 0.13
8	16.7	1.92 ± 0.04	0.08 ± 0.01	2.1 ± 0.35
10	20	1.86 ± 0.02	0.10 ± 0.01	1.87 ± 0.3
12	23.1	1.83 ± 0.01	0.11 ± 0.01	1.87 ± 0.3
14	25.9	1.80 ± 0.01	0.08 ± 0.01	1.4 ± 0.2

Table S2. Secondary thin film HfZrTaMoWC$_{1-x}$ sample set including methane parameters during deposition, thickness, film density, electrical conductivity, thermal conductivity and heat capacity.

CH_4 Flow Rate	% CH_4	Thickness	Density	Electrical Conductivity	Thermal Conductivity	Heat Capacity
(sccm)		(nm)	(g cm^{-3})	($\mu\Omega^{-1}\cdot m^{-1}$)	($W\cdot m^{-1}\cdot K^{-1}$)	(J cm^{-3} K^{-1})
2	4.8	83.6	11.73	0.46 ± 0.01	4.0 ± 0.6	2.1 ± 0.6
4	9.1	96.4	9.68	0.19 ± 0.01	2.8 ± 0.3	2.7 ± 0.6
6	13	100	9.23	0.11 ± 0.01	2.9 ± 0.15	3.1 ± 0.6
8	16.7	100.8	9	0.12 ± 0.01	2.6 ± 0.4	2.9 ± 0.6
10	20	103.3	8.14	0.12 ± 0.01	1.9 ± 0.3	2.9 ± 0.6
12	23.1	102.8	7	0.11 ± 0.01	1.8 ± 0.3	2.6 ± 0.6
14	25.9	92.3	6.77	0.09 ± 0.01	1.7 ± 0.3	2.3 ± 0.6

S3. Analysis of an additional HEC composition $HfZrTaTiNbC_{1-x}$

The ~100 nm thick $HfZrTaTiNbC_{1-x}$ films were synthesized by using reactive radio frequency (RF) sputtering at 200 watts. We used an equimolar 99.5% HfNbTaTiZr alloy target as a source of metal where 99.99% CH4 was used as a C source. An ultra-high purity (99.999%) Ar was used as sputtering gas and a constant flow rate of 20 sccm was maintained for all the deposition. Thin films were deposited on the c-plane sapphire substrate at a temperature of 650 °C and the total pressure during deposition was fixed at 5 mT. Thermal conductivities and similar electron and phonon thermal conductivity analyses for these films as those in the main manuscript are shown in Figs. S2 and S3.

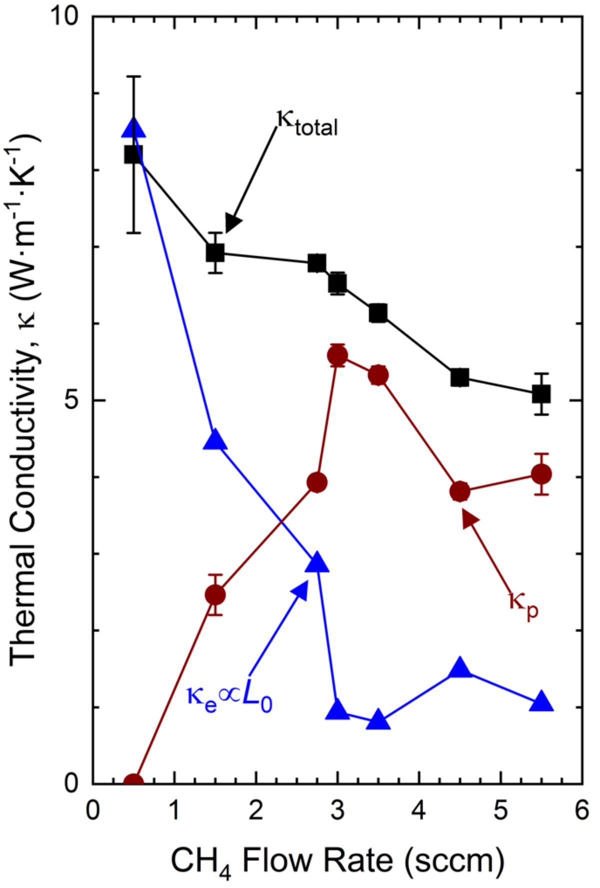

Figure S2: Thermal conductivity of $HfZrTaTiNbC_{1-x}$ thin films measured with TDTR (κ_{total}) plotted as a function of percent methane flow rate in the deposition plasma. The electrical contributions to the measured total thermal conductivity, κ_e, are calculated from the Wiedemann-Franz Law applied to electrical resistivity measurements on these films assuming the low temperature value for $L = L_0 = 2.44 \times 10^{-8}$ W Ω K^{-2}, and thus in this figure, $\kappa_e \propto L_0$. The phonon contribution to these $HfZrTaTiNbC_{1-x}$ thin films' thermal conductivities are then calculated as $\kappa_p = \kappa_{total} - \kappa_e$. Similar trends in the electronic and phononic thermal conductivities are observed in this HEC composition as the HEC films reported in the main manuscript (Figs. 2 and 3).

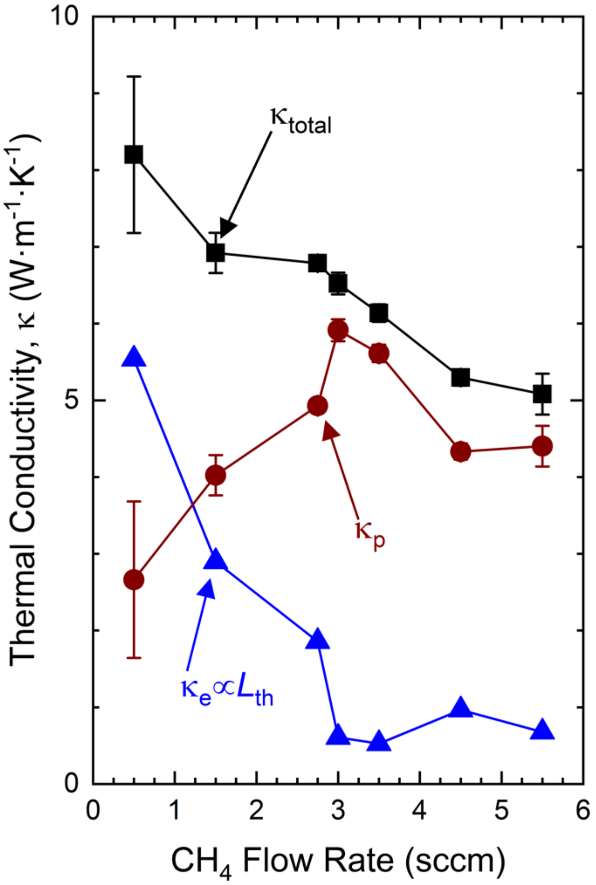

Figure S3: Same as Fig. S2 only with κ_e calculated with the Lorentz number that accounts for inelastic electron-phonon scattering and electron-impurity scattering given by Eq. 1 in the main manuscript and discussed therein. Similar trends are observed here in κ_e and κ_p as in Fig. S4, in that we observe a cross-over from electron-dominated thermal conductivity to phonon-dominated thermal conductivity with increased methane flow rate in the deposition plasma regardless of our assumption of the Lorentz number used in our Wiedemann-Franz Law calculations.

S4. Density functional theory (DFT)

The density functional theory (DFT) calculations were carried using the projector augmented wave (PAW)[13,14] method as implemented in the Vienna Ab initio Simulation Package (VASP).[14-16] The generalized gradient approximation as parameterized by Perdew et al. was used for the exchange-correlation potential,[17] and the standard PAW potentials, supplied with the VASP 4.6 package, were also used.[18] A cut-off energy of 520 eV was used for the plane wave basis, and convergence was assumed when the energy difference between two consecutive self-consistent cycles was less than 2 meV. The Brillouin-zone was sampled by a Γ-centered mesh of 8 X 4 X 2 k points. The defect-free HEC6 unit cell contained 40 carbon and 40 atoms in a rocksalt structure. The latter were randomly arranged on the cation fcc sublattices within the rocksalt lattice using the special quasi-random structure algorithm.[19] To create a system with 5% and 10% vacancy concentrations, two and four carbon atoms were randomly removed, respectively, from the defect-free system. Similarly, two and four carbon atoms were randomly added to interstitial sites of the ideal system to create carbon-rich systems with 5% and 10% interstitials. After the energy of each system was minimized with respect to atom positions and unit cell size, the electrical resistivity was calculated by solving the Boltzmann transport equation within the constant relaxation time approximation using the BoltzTraP code.[20] A relaxation time of 4.2×10^{-15} seconds as was previously reported for NbC was used here. The electronic contributions to the thermal conductivity were calculated assuming Wiedemann–Franz behavior, as was done for the experimental data. For graphite, the binding energy was calculated from DFT as described above using a hexagonal structure with 80 carbons in the unit cell.[21]

S5. Supplemental references

1. Y. Zhang, T. T. Zuo, Z. Tang, M. C. Gao, K. A. Dahmen, P. K. Liaw and Z. P. Lu, "Microstructures and properties of high-entropy alloys," *Progress in Materials Science* **61**, 1-93 (2014).
2. A. J. Schmidt, "Pump-probe thermoreflectance," *Annual Review of Heat Transfer* **16**, 159-181 (2013).
3. D. G. Cahill, "Analysis of heat flow in layered structures for time-domain thermoreflectance," *Review of Scientific Instruments* **75**, 5119-5122 (2004).
4. P. E. Hopkins, "Thermal transport across solid interfaces with nanoscale imperfections: Effects of roughness, disorder, dislocations, and bonding on thermal boundary conductance," *ISRN Mechanical Engineering* **2013**, 682586 (2013).
5. E. F. Westrum and G. Feick, "Zirconium Carbide: Heat Capacity and Thermodynamic Properties from 5 to 350° K," *Journal of Chemical & Engineering Data* **8**, 176-178 (1963).
6. E. F. Westrum and G. Feick, "Heat capacities of HfB2.035 and HfC0.968 from 5 to 350 K," *The Journal of Chemical Thermodynamics* **9**, 293-299 (1977).
7. E. F. Westrum and J. A. Sommers, "Heat capacity of hafnium mononitride from temperatures from 5 to 350 K," *Journal of Thermal Analysis and Calorimetry* **69**, 103-112 (2002).
8. Y. S. Touloukian and E. H. Buyco, *Thermophysical Properties of Matter - Specific Heat: Metallic Elements and Alloys* (New York, IFI/Plenum, 1970).
9. Y. S. Touloukian, R. W. Powell, C. Y. Ho and P. G. Klemens, *Thermophysical Properties of Matter - Specific Heat: Nonmetallic Solids* (New York, IFI/Plenum, 1970).
10. Y. S. Touloukian, R. W. Powell, C. Y. Ho and P. G. Klemens, *Thermophysical Properties of Matter - Thermal Conductivity: Nonmetallic Solids* (New York, IFI/Plenum, 1970).
11. A. Giri, J.-P. Niemel\"a, C. J. Szwejkowski, M. Karppinen and P. E. Hopkins, "Reduction in thermal conductivity and tunable heat capacity of inorganic/organic hybrid superlattices," *Physical Review B* **93**, 024201 (2016).
12. R. M. Costescu, M. A. Wall and D. G. Cahill, "Thermal conductance of epitaxial interfaces," *Physical Review B* **67**, 054302 (2003).
13. P. E. Blochl, O. Jepsen and O. K. Andersen, "Improved tetrahedron method for Brillouin-zone integrations," *Physical Review B* **49**, 16223-16233 (1994).
14. G. Kresse and J. Furthmüller, "Efficiency of ab-initio total energy calculations for metals and semiconductors using a plane-wave basis set," *Computational Materials Science* **6**, 15-50 (1996).
15. G. Kresse and J. Furthmüller, "Efficient iterative schemes for ab initio total-energy calculations using a plane-wave basis set," *Physical Review B* **54**, 11169-11186 (1996).
16. G. Kresse and J. Hafner, "Ab initio molecular dynamics for liquid metals," *Physical Review B* **47**, 558-561 (1993).
17. J. P. Perdew, K. Burke and M. Ernzerhof, "Generalized Gradient Approximation Made Simple," *Physical Review Letters* **77**, 3865-3868 (1996).
18. Z. Rak, C. M. Rost, M. Lim, P. Sarker, C. Toher, S. Curtarolo, J. P. Maria and D. W. Brenner, "Charge compensation and electrostatic transferability in three entropy-stabilized oxides: Results from density functional theory calculations," *Journal of Applied Physics* **120**, 095105 (2016).
19. A. Zunger, S. H. Wei, L. G. Ferreira and J. E. Bernard, "Special quasirandom structures," *Physical Review Letters* **65**, 353-356 (1990).

20. G. K. H. Madsen and D. J. Singh, "BoltzTraP. A code for calculating band-structure dependent quantities," *Computer Physics Communications* **175**, 67-71 (2006).
21. N. W. Ashcroft and N. D. Mermin, *Solid State Physics* (Saunders College, Fort Worth, 1976).